UNDERLYING TECHNOLOGY PROGRAMME 2005

PHYSICS INTEGRATION

TASK: UT-TPDC-IRRCER
IRRADIATION EFFECTS IN CERAMICS FOR HEATING AND CURRENT DRIVE, AND DIAGNOSTIC SYSTEMS

***Deliverables*: A. UV-visible spectral behaviour of sapphire optical fibres under gamma-ray and neutron radiation and B. Investigations on the gamma-ray and electron beam radiation effects on semiconductor optical detectors for sensing and optical communication applications**

D. Sporea, Adelina Sporea*, C.Oproiu*, B. Constantinescu**, and I. Vata***

**National Institute for Laser, Plasma and Radiation Physics, Magurele*
***"Horia Hulubei" National Institute of R&D for Physics and Nuclear Engineering, Magurele*

A. UV-visible spectral behaviour of sapphire optical fibres under Gamma-ray and neutron radiation

1. Introduction

Optical components (windows, mirrors) as well as optical fibres will play a major role in plasma diagnostics and remote handling in ITER-like fusion reactors, as they will have to carry optical signal in a hostile environment (high dose rate and total doses gamma-rays irradiation, high neutron fluence, electromagnetic noise, high temperature, etc.). Such components have to be tested under extreme operating conditions in order to estimate their possible use in ITER and future DEMO installations. Generally, silica optical fibres exhibit a poor optical transmission in the UV-visible spectral range as colour centres are already present in the optical fibber core or as they are developed during ionizing irradiation.

An alternative to silica optical fibres can be sapphire optical fibres which were very recently introduced on the market. As compared to silica optical fibres, the sapphire ones have a very good optical transmission from about 400 nm to 2.5 μn, with an exceptional temperature resistance (up to 1200 ^{O}C).

The present report is related to the evaluation of the degradation of the optical attenuation in the UV-visible spectral range for sapphire optical fibres, subjected to ***gamma-ray and neutron*** irradiation, to asses their possible use for plasma diagnostics in fusion installations (i.e. ITER), investigations performed during 2005.

2. Results concerning the irradiation of sapphire optical fibers

The investigated sapphire optical fibres are commercially available products having a core diameter of 425 μm and a length of 25 cm. The fibres have no cladding or jacket. The fibre ends were polished by the manufacturer. Removable SMA 905 connectors were used during the measurement of the spectral attenuation.

The spectral optical attenuation of the fibres, before and after each irradiation step, was measured over the 200 nm to 1700 nm spectral range using:

a) a fibre optic spectrometer with a spectral resolution of 1 nm and an entrance slit of 10 μm in connection with a deuterium lamp (output power stability of 0.05 % p-p and a drift of +/- 5%/h), for the 200 nm – 650 nm range;

b) a fibre optic spectrometer with a spectral resolution of 0.5 nm and an entrance slit of 5 μm in connection with a tungsten lamp (output power stability of 0.05 % p-p), for the 650 nm – 850 nm range;

c) a fibre optic spectrometer with a spectral resolution of 0.5 nm and an entrance slit of 5 μm in connection with a tungsten lamp (output power stability of 0.05 % p-p), for the 850 nm – 1050 nm range;

d) an optical spectrum analyzer (OSA) with a spectral resolution of 0.05 nm in connection with a tungsten halogen (output power stability of +/- 0.05 dBm at 20 ^{O}C), for the spectral range of 650 nm – 1700 nm.

For a better coupling, the optical fibre silica probes used to connect the sapphire sample to the instrumentation have a 400 μm core diameter, for the cases ***a-c*** mentioned above. In the case ***d***, when the OSA was employed, the sapphire optical fibre was coupled to the instrument input through a 62.5 μm core diameter silica fibre in order to set the required spectral resolution.

A dedicated virtual instrument was designed to be used in order to evaluate the spectral attenuation with the optical fibre spectrometer. In this case, the spectral attenuation is computed with the formula:

$$A_\lambda = -10\log_{10}\left(\frac{S_\lambda - D_\lambda}{R_\lambda - D_\lambda}\right), \qquad (1)$$

where, A_λ represents the spectral optical attenuation (dB); S_λ – the spectral distribution of the signal measured by the spectrometer as the light is passing through the sample optical fibre; D_λ – the spectral distribution of dark signal measured by the spectrometer; R_λ – the spectral distribution of deuterium/ tungsten lamps output, measured by the spectrometer.

In the case of the optical spectrum analyzer the spectral attenuation is computed according to:

$$A_\lambda = \left(\frac{R_\lambda - S_\lambda}{R_\lambda / S_\lambda} \right), \qquad (2)$$

where, A_λ represents the spectral optical attenuation (dB); S_λ – the spectral distribution of the signal measured by the optical spectrum analyzer as the light is passing through the sample optical fibre; R_λ – the spectral distribution of incandescent lamps output, measured by the optical spectrum analyzer.

All the acquired data were saved in an Excel compatible format for further processing. As the measurements are subjected to an arbitrary bias signal introduced by the connecting set-up (connectors, optical fibre probes) the post acquisition processing implies the compensation of both this bias and the contribution of the connecting optical fibres to the measured optical attenuation.

In order to study the irradiation-induced effects in sapphire optical fibres, different optical fibre samples were subjected to gamma-ray, neutron, electron beam and proton beam irradiation. We performed proton irradiation in addition to the planned gamma and neutron irradiation because the dose rate at gamma-ray is too low to produce radioluminescence in the sample fibre. All the irradiation and measurements were done off-line, at room temperature. Exceptions were some measurements during proton irradiation, done in situ for radioluminescence investigations.

The irradiations were done as follows:

A. gamma-ray irradiation at the ^{60}Co gamma facility of the "Horia Hulubei" National Institute of R&D for Physics and Nuclear Engineering–IFIN-HH, at a dose rate of 0.33 kGy/h, and the total irradiation dose of 536 kGy;
B. neutron irradiation at the Cyclotron accelerator of the "Horia Hulubei" National Institute of R&D for Physics and Nuclear Engineering–IFIN-HH, using a deuteron beam incident on a Be target, producing neutrons with an energy of about 5.2 MeV. The neutrons flux above 1 MeV is estimated with a relative error of about 20 %. The measured production yield, at 10 cm distance from Be target, is 2.13×10^8 n.cm^{-2}.s^{-1}.μA^{-1}. The maximum neutron flux achievable in our set-up, at a distance of 10 cm from the target, is 2.10^9 n.cm^{-2}.s^{-1}.μA, corresponding to a deuteron beam intensity of 10 μA. In practice, a neutron fluence up to 10^{13} n.cm^{-2} can be obtained in about 1-6 days of irradiation, depending of the position of the samples.
C. electron beam irradiation at the linear accelerator of the National Institute for Laser, Plasma and Radiation Physics, 3 μs/ 100 Hz pulsed operation, with a dose rate of 2 kGy/min, a total dose of 25 kGy, and beam diameter of 10 cm;
D. proton irradiation at the Tandem irradiation facility of the "Horia Hulubei" National Institute of R&D for Physics and Nuclear Engineering–IFIN-HH, with a beam current of 1 nA, dose rate of 200 Gy/s, a total dose of 6.27 MGy, the proton energy of 14 MeV, and the beam diameter of about 3 mm.

In the case of gamma irradiation the optical fiber was uniformly exposed along 25 cm, while for neutron irradiation the uniform flux was over 10 cm length.

Before any irradiation all the available sapphire optical fibre samples were measured over the entire spectral range (Figures 1 to 4). As expected for sapphire components, not all the samples have a very good transmission in the UV spectral range. Some optical fibres have a high attenuation in the UV below 300 nm, while others can be used only above 500 nm. For comparison, the optical attenuation of the connecting optical fibre probes was also illustrated. In this case, the probes were a high OH content silica optical fibres, of solarization resistant type. It is important to notice:

- the small influence of the connecting fibres in the UV range (below 300 nm);
- the very low optical attenuation of all fibres in the visible and IR range;
- the attenuation peak introduced by the optical fibre probes in the near-IR region (at about 960 nm).

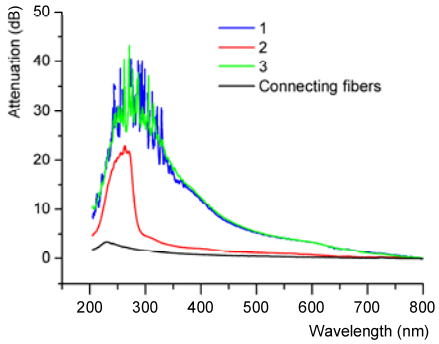

Figure 1. The optical attenuation of three sapphire optical fibres (denoted by 1-3) and the connecting silica optical fibre probes (the black trace), measured over the UV-visible spectral range.

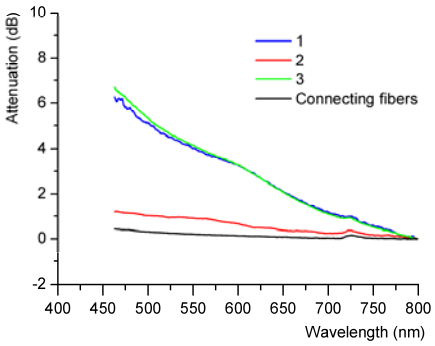

Figure 2. The optical attenuation of three sapphire optical fibres (denoted by 1-3) and the connecting silica optical fibre probes (the black trace), measured over the visible and near-IR spectral range.

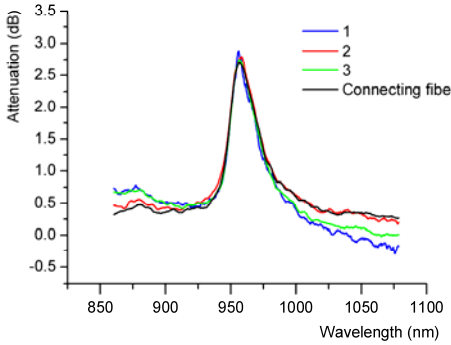

Figure 3. The optical attenuation of three sapphire optical fibres (denoted by 1-3) and the connecting silica optical fibre probes (the black trace), measured over the near-IR spectral range.

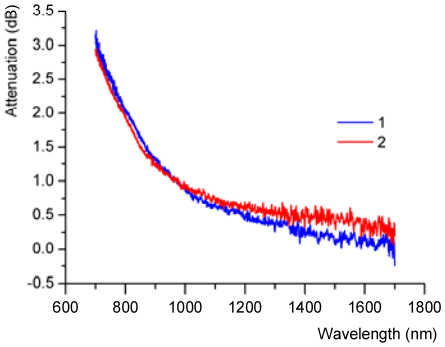

Figure 4. The optical attenuation of two sapphire optical fibres (denoted by 1-2), measured over the IR spectral range with the optical spectrum analyzer.

The sapphire optical fibres proved to have a very good radiation resistance as small changes in the optical absorption can be observed after all types of irradiations (Figures 5 – 7).

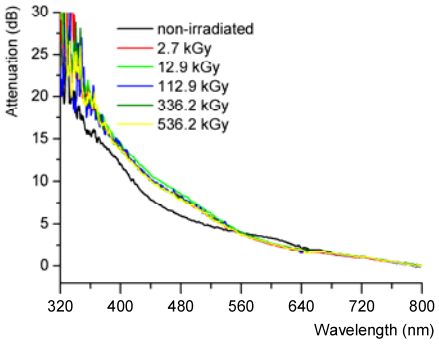

Figure 5. The optical attenuation of the sapphire optical fibre subjected to gamma-ray irradiation.

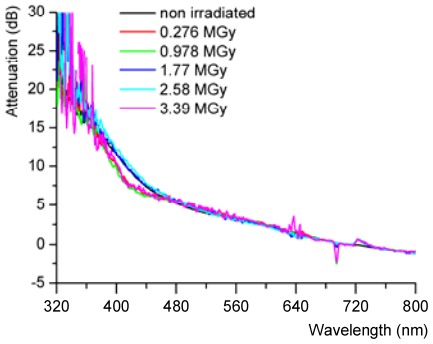

Figure 6. The optical attenuation of the sapphire optical fibre subjected to proton irradiation.

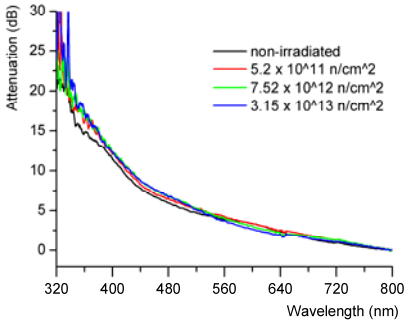

Figure 7. The optical attenuation of the sapphire optical fibre subjected to neutron irradiation.

It is important to notice the radioluminescence signal generated during proton irradiation (Figure 8).

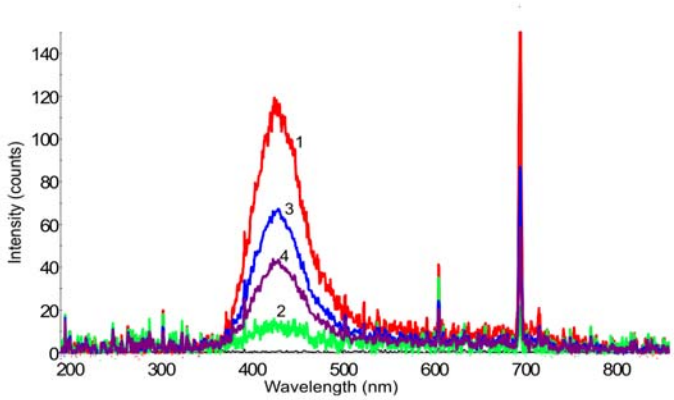

Figure 8. The radioluminescence emission from a sapphire optical fibre, for proton beam irradiation, at the total irradiation doses of: 1 – 1.32 MGy; 2 – 2.076 MGy; 3 – 2.91 MGy; 4 – 3.324 MGy.

3. Conclusions

Following the irradiation of sapphire optical fibres very small changes of the optical attenuation can be noticed in the spectral band 450 - 500 nm after gamma irradiation. Neutron, electron beam and proton irradiation produces no significant changes. A slight increase of the attenuation appears after neutron irradiation as a peak at about 1380 nm. [1]

In situ proton irradiation indicates three emission radioluminescence bands at 450 nm, 605 nm and 695 nm. The radioluminescence signal is a fluctuating one, being more intense at the beginning of the irradiation. When the irradiation is continued after a short break (20 minutes) the radioluminescence signal has an amplitude almost equal to that present before the interruption of the irradiation process.

4. Collaborative actions in relation to irradiation effects on optical fibres

Task: Investigation on the irradiation effects in optical fibers in the UV spectral range

Partner: Association EURATOM - The Belgian State (Centre d'Etude de l'Energie Nucleaire – SCK/CEN Mol)

The investigations were carried out both on-line and off-line. [2], [3] The optical fibres were irradiated in most cases in Romania, while only one optical fibre was irradiated at Mol and measured in the Laser Metrology and Standardisation Laboratory. All the measurements were done at room temperature, focusing on the assessment of the increase of the optical absorption in the UV spectral range. The measurements were done with a set-up developed in the Romanian Laboratory, set-up controlled by a PC through proprietary software developed under the graphical programming environment LabVIEW. The irradiation included gamma-ray, neutron, proton, and electron beam.

A. Off-line irradiation conditions:

a) Neutron irradiation irradiation conditions:

- deuteron beam on a Be target: 13 MeV
- beryllium target of 165 mg.cm^{-2} thickness
- samples are located downstream at the distances from 10 to 40 cm from the Be target
- the maximum neutron flux at a distance of 10 cm from the target, is 2.10^{9} n.cm^{-2}.s^{-1}.μA^{-1}, corresponding to a deuteron beam intensity of 10 μA
- irradiation was performed at room temperature

b) Proton irradiation irradiation conditions:

- energy: 15 MeV; current intensity: 1 nA; dose rate 200 Gy/s (5 x 10^{9} protons/s); irradiation zone: 2 mm and room temperature

c) Electron-beam irradiation irradiation conditions:

- mean electron energy: 7 MeV; electron beam current 1- 4 μA; pulse repetition rate 100 Hz; pulse duration 3.5 μs; beam transversal area 100 cm^{2}; spot uniformity ± 5 %; dose rate: 2 kGy/min and room temperature

B. On-line irradiation conditions:

a) Proton irradiation irradiation conditions

The same conditions as above. Dose rate 200 Gy/s (**6 x 10^9 protons/s**)

b) Gamma irradiation irradiation conditions:

- ^{60}Co source; dose rate 5.3 kGy/h;

- irradiation was performed at room temperature, in a hot cell in air;
- radial distance from the source: 5.3 cm;

The length of the irradiated optical fibre: 4.5 m. The fibre was coiled to 13.5 cm diameters

Irradiated optical fibres: KS 4v type fibre, 200 μm core diameter; deep UV type fibre, 400 μm core diameters, SSU1.1 type fibre, 600 μm core diameter. Some of the results are given in Figures 9 – 10.

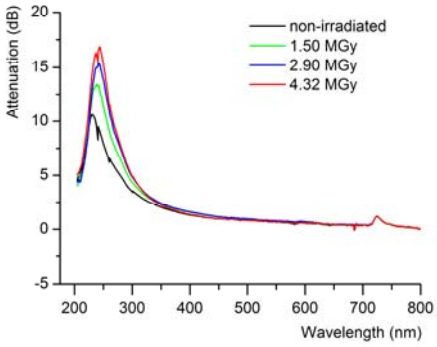

Figure 9. Fibre deep UV subjected to in situ - proton irradiation.

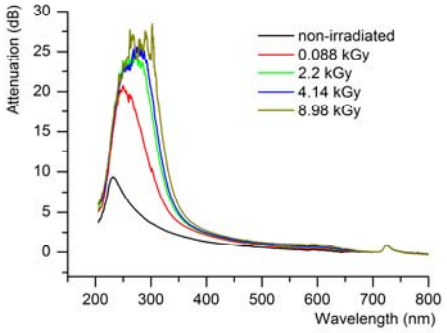

Figure 10. Fibre 3- SSU1.1 subjected to in situ - gamma irradiation

It has to be noticed that gamma-ray irradiation produces a much broadening of the optical absorption spectrum than the proton irradiation. The same is the case for gamma irradiation as compared to neutron irradiation.

The co-operation will continue in the future on:

- the evaluation of other types of optical fibres of interest for their use for plasma in ITER
- the assessment of colour centre dynamics under different irradiation conditions.

References

[1] **Sporea D., Sporea Adelina** "*Radiation effects in sapphire optical fibres*", accepted to be presented at the 10th European Conference on Defects in Insulating Materials (EURODIM 2006), Milano, July 2006.

[2] **Sporea D., Sporea Adelina**, "*Evaluation of Solarization Resistant Optical Fibers under Gamma-Ray Irradiation and Temperature Stress",* presented at the Workshop on Fibres and Optical Passive Components, Palermo, Italy, June 2005.

[3] **Sporea D., Sporea Adelina, Constantinescu B.**, "*In-situ Measurements of Optical Fibers under Gamma-ray Irradiation*", presented at the 12th International Conference on Fusion Reactor Materials, Santa Barbara, California, USA, December 2005.

B. Investigations on the gamma-ray and electron beam radiation effects on semiconductor optical detectors for sensing and optical communication applications

1. Introduction

The present report refers to the evaluation, during 2005, of the degradation of the electrical and optoelectronic characteristics of semiconductor photodiodes, subjected to ***gamma-ray and electron beam*** irradiation, to asses their possible use in sensing and communications systems, for fusion installations (i.e. ITER).

2. Results

2.1 Irradiation and measuring condition

Considering the possible applications of semiconductor photodiodes in fusion installations (sensing devices, optical free space or optical fibre-based communications, robotic systems, etc.), we investigated three types of photodiodes as they were subjected to gamma-ray and electron beam irradiation. Four of the evaluated photodiodes were Si photodiodes, while the other two were InGaAs photodiodes. In the case of the Si photodiodes two of them have a large detecting area (3 mm x 3 mm) susceptible to be used in sensing and positioning applications, and the other two have a small detecting area of 0.991 mm diameter. The InGaAs detectors have a diameter of the detecting area equal to 0.3 mm. The characteristics and the designation of these photodiodes as they are presented in this report are given in Table 1.

Table 1. The characteristic of the investigated photodiodes

Photodiode designation/ Characteristics	**Ph 1 (2)**	**Ph 3 (4)**	**Ph 5 (6)**
Material	Si	Si	InGaAs
Sensing area (mm)	□ = 3 x 3	Φ = 0.991	Φ = 0.3
Capacitance (pF)	-	5.2 (V_R = 3.3 V)	5
Max. reverse voltage (V)	30	20	15
Max. reverse current (mA)	-	-	5
Max. Forward current (mA)	-	-	25
Responsivity (A/W)	30 nA/lx	0.5	0.9 (1310 nm) 0,95 (1550 nm)
Dark current (nA)	50	0.3	6
NEP ($W/Hz^{1/2}$)	-	-	6.28×10^{-15}
Rise/ fall time (ns)	100 ms	1200	1.5

From each type of photodiode, one was subjected to either gamma or electron beam irradiation. The photodiodes designated with Ph 1, Ph 3, and Ph 5 were irradiated by gamma rays, while the photodiodes denoted by Ph 2, Ph 4, and Ph 6 were irradiated by electron beam. The photodiodes pairs 1 and 2, 3 and 4, 5 and 6 are of the same type.

The photodiode 1 and 2 have a metallic T-18 case with a flat glass window. The photodiodes 3-6 are packed into metallic FC, flange type, receptacle package without any window, ready to be used with optical fibre patch cords. All the photodiodes designed for communication applications (detectors 3-6) have also a pin connected to the case, while the large area detectors have only two terminals.

The photodiode characteristics evaluated during this campaign are:

- the dark current;
- the spectral responsivity at different wavelengths;
- the turn-on and turn-off time.

The spectral responsivity was evaluated by exposing the photodiode to the radiation of different laser diodes emitting in the visible and near-IR spectral region. The semiconductor lasers employed for the characterization of the spectral and spatial responsivity emit optical radiation at the following wavelengths:

- for the photodiodes 1- 4 we used laser diodes operating at: 653 nm, 650 nm, 670 nm, 780 nm, 808 nm and 850 nm;
- for the photodiodes 5 and 6 the laser diodes used emitted at 808 nm, 850 nm, 1310 nm and 1550 nm.

All the laser diodes used have a free-space propagation beam. For this reason the laser beams were either collimated by appropriate optical systems or were coupled to the detector using an integrating sphere. The measurements were carried out in a dark room, under a steady-state ambient illumination lower than 0.3 μW optical radiation equivalent. The laser diodes were controlled by a laser diode driver/ temperature controller. In this way, a high stability of the optical signal was achieved. The semiconductor lasers were operated in both constant optical power and constant current of the internal monitoring photodetector. The optical power of each laser diode was monitored over 5 minutes by a precision laser power meter, in order to assess the stability of its emitted power. In the case of large area detectors the spatial responsivity of the photodiode along two perpendicular axes was also measured at different laser wavelengths. For each photodiode two irradiation sessions took place. All the investigated parameters were measured both before and after each irradiation step. Each photodiode, when measured, was connected to a precision current-to-voltage converter amplifier, with variable gain. The measurements and the irradiation were done at room temperature. The parameters of this amplifier are given in Table 2. The amplified signal generated at the amplifier output was coupled to the input of a digital-to-analogue converter. Data from the converter was picked up by a PC via an USB connection.

For turn-on and turn-off time measurements the laser diodes were switched on and off by a manual command, and the transient response of the investigated photodiode and current-to-voltage converter assembly was estimated. In this situation, the overall temporal

response was limited by the amplifier bandwidth, the laser commutation performances and the rate of the data conversion.

Table 2. The parameters of the current-to-voltage amplifier

Parameter	Units	Value
Transimpedance	V/A	1 x 10^3…1 x 10^{11}
Gain Accuracy	%	± 1
Gain Drift	%/^{O}C	0.01% (10^6); 0.01% (10^7); 0.01% (10^8); 0.02% (10^9);
Lower Cut-Off Frequency	Hz	DC / 1
Upper Cut-Off Frequency	kHz	Max. 500 (switchable to 10 Hz)
Equ. Input Noise Current	fA	130 (10^6); 43 (10^7); 13 (10^8); 4.3 (10^9)
Equ. Input Noise Voltage	nV/√Hz	4
Input Offset Current Drift	pA/ ^{O}C	27 (10^6); 2.5 (10^7); 0.2 (10^8); 0.06 (10^6)
Input bias Current	pA	1
Bias Voltage Range	V	± 10 (max.22 mA, switchable to GND)

All the measurements were performed over 3-5 minutes intervals and the data were averaged over these time periods in order to reject the noise which can be picked-up across the wiring system. In this way, the signal-to noise (S/N) ratio is much improved. During the measurements the photodiode biasing was kept to 0 V, to minimize the dark current.

In the case of large area photodiodes the laser beam was focused in the detecting plane at about 0.8-1.1 mm spot diameter. The optical setup in such a situation is presented in Figure 1. Before each measurement of the photodiode spectral responsivity the laser optical power was measured with a Si detector embedded into an integrating sphere. In this way, all the emitted optical power is captured and evaluated. The programmed to control the laser power meter through the GPIB interface was developed in the Laboratory. Data can be acquired with either a 0.5 Hz or a 3 Hz rate and the results can be saved as Excel files for processing. During the acquisition the mean, maximum and minimum values are computed and displayed. Each time the laser diode changes its wavelength, as it was measured by a wavelength meter, the wavelength value is entered as in input parameter into the laser power meter to make the appropriate spectral correction of the calibration.

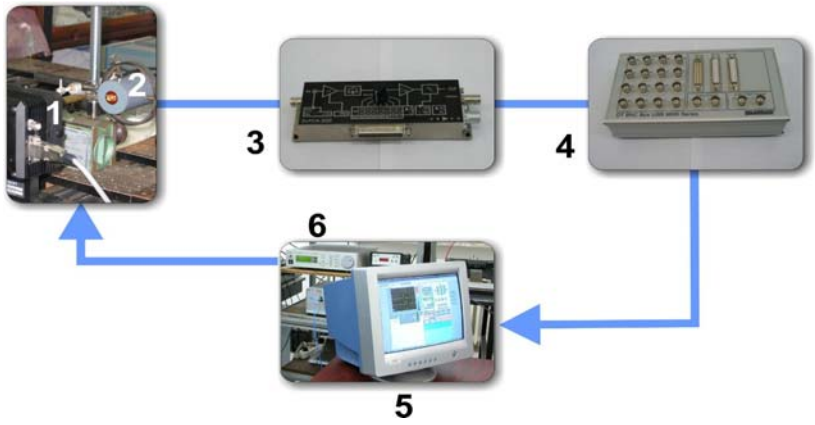

Figure 1. The setup for the responsivity measurements for large area photodiode: 1 – laser diode mount and the laser diode; 2 – photodiode mount and the photodiode; 3 – current-to-voltage converter; 4 – data acquisition board; 5 – PC; 6 – laser driver/ temperature controller.

The spectral responsivity of the small area Si photodiodes (items 3 and 4) was evaluated using the setup illustrated in Figure 2. The laser beam of the laser diode was focused in the input plane of an integrating sphere, while the detecting plane of the photodiode to be investigated was kept at the output port of the integrating sphere and the current generated by the optical radiation incident on the detector was acquired.

In the first step of the process, the photodiode to be evaluated was replaced by the photodiode # 1 for which the responsivity at each wavelength was previously determined using the setup in Figure 1. In the second step, the light exiting the integrating sphere was used to expose the detecting area of photodiodes 3 and 4. In this way, a calibration of the measuring setup was implemented.

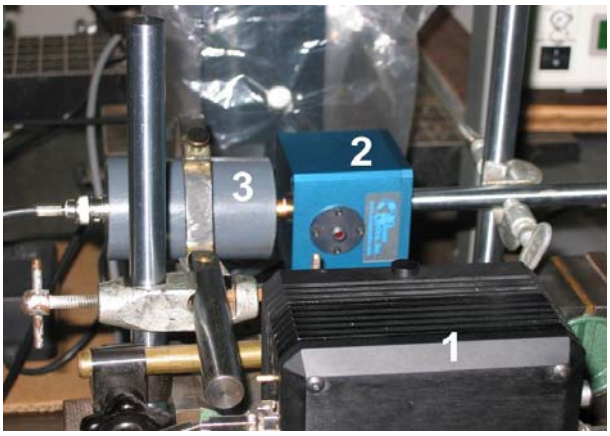

Figure 2. The setup for the evaluation of the spectral responsivity of small area Si photodiodes: 1 – semiconductor laser temperature mount; 2 – integrating sphere operating in the visible range; 3 – the mounting of the Si photodiode.

In order to determine the spectral responsivity of the photodiodes # 5 and 6 (InGaAs), a third integrating sphere operating in the IR spectral range was used. The beam of the laser diode was coupled to the input port of the integrating sphere, while the photodiode to be evaluated (# 5 or 6) was placed at the integrating sphere output port. In the mean time, the integrating sphere uses a second calibrated photodetector embedded inside the sphere, photodetector employed to evaluate the incident laser optical power (Figure 3).

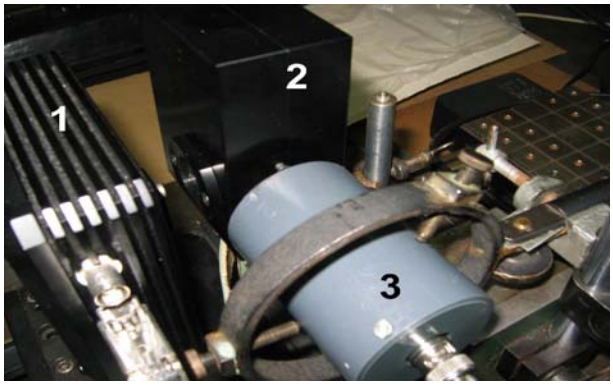

Figure 3. The setup for the evaluation of the spectral responsivity of small area InGaAs photodiodes. 1 – semiconductor laser temperature mount; 2 – integrating sphere operating in the infrared range; 3 – the mounting of the InGaAs photodiode.

For the laser diodes emitting at 808 nm and 850 nm their wavelength was determined with a wavelength meter, while in the case of laser diodes emitting at communication wavelengths (1310 nm and 1550 nm) their wavelength was evaluated with an optical spectrum analyzer. The values for these wavelengths were entered as in input parameter into the laser power meter for spectral correction of the calibration.

For small area photodiodes the use of an integrating sphere assures a uniform illumination of the sensing area, which is completely filled. So, the reproducibility of the measurements is kept at a high level.

The software used to acquire and to save data from the converter was a dedicated one, offered by the data acquisition board manufacture. Data can be saved either in an Excel compatible format or as screen pictures. The programmed was used to acquire data related to: the spectral responsivity, spatial responsivity, dark current, and the switch off/on time. The saved data can be further processed.

2.2 Results concerning the irradiation of semiconductor photodiodes

The above mentioned photodiodes were irradiated by gamma-rays and electron beams, separately. The total irradiation doses are given in each case in Table 3.

Table 3. The total irradiation doses to which each photodiode was subjected.

Photodiode/ Irradiation step	**Ph 1**	**Ph 2**	**Ph 3**	**Ph 4**	**Ph 5**	**Ph 6**
Total gamma dose (kGy) – step 1	-	90	-	90	-	90
Total gamma dose (kGy) – step 2	-	100	-	100	-	100
Total electron beam dose (kGy) – step 1	100	-	100	-	100	-
Total electron beam dose (kGy) – step 2	200	-	200	-	200	-

Detailed data on the irradiation induced changes on the operating parameters of various laser diodes under different irradiation conditions can be found in the 2005 Final Report of the task, where data are presented in over 30 graphs.

In the tables 4-9 the changes induced by gamma irradiation as it concerns the photodiodes dark current are presented. For each situation (non-irradiated photodiode, different total irradiation doses) the mean values of the signal at the output of the current–to-voltage converter were computed and they are indicated along with the standard deviation at 3 σ. In each situation the converter gain is specified. The change of the dark current after irradiation is calculated by dividing the difference between the final value and the initial value (for the non-irradiated photodiode) by the initial value and multiplying the result by 100. A change is considered positive if the output voltage increases with respect to the initial value, and is considered negative as the final value decreases with respect to the initial value.

Table 4. The change of the photodiode Ph1 dark signal after electron beam irradiation.

Total dose (kGy)	Mean value (mV)/ $A=10^6$ V/A	Standard deviation (95 %)	Mean value (mV)/ $A=10^6$ V/A	Standard deviation (95 %)	Mean value (mV)/ $A=10^6$ V/A	Standard deviation (95 %)	Change (%)
0	- 1.40	0.09	-	-	-	-	0
100	-	-	- 1.27	0.07	-	-	+ 9.65
300	-	-	-	-	- 1.85	0.06	- 31.35

Table 5. The change of the photodiode Ph2 dark signal after gamma irradiation.

Total dose (kGy)	Mean value (mV)/ $A=10^6$ V/A	Standard deviation (95 %)	Mean value (mV)/ $A=10^6$ V/A	Standard deviation (95 %)	Mean value (mV)/ $A=10^6$ V/A	Standard deviation (95 %)	Change (%)
0	- 1.18	0.06	-	-	-	-	0
90	-	-	- 0.28	0.07	-	-	+ 76.00
190	-	-	-	-	- 1.69	0.06	- 43.45

Table 6. The change of the photodiode Ph3 dark signal after electron beam irradiation.

Total dose (kGy)	Mean value (mV)/ $A=10^8$ V/A	Standard deviation (95 %)	Mean value (mV)/ $A=10^8$ V/A	Standard deviation (95 %)	Mean value (mV)/ $A=10^8$ V/A	Standard deviation (95 %)	Change (%)
0	36.38	16.20	-	-	-	-	0
100	-	-	10.50	7.77	-	-	- 71.13
300	-	-	-	-	- 5.04	4.11	- 113.86

Table 7. The change of the photodiode Ph4 dark signal after gamma irradiation.

Total dose (kGy)	Mean value (mV)/ $A=10^7$ V/A	Standard deviation (95 %)	Mean value (mV)/ $A=10^7$ V/A	Standard deviation (95 %)	Mean value (mV)/ $A=10^7$ V/A	Standard deviation (95 %)	Change (%)
0	27.02	3.54	-	-	-	-	0
90	-	-	2.14	0.89	-	-	- 92.06
190	-	-	-	-	- 1.69	0.47	- 106.27

Table 8. The change of the photodiode Ph5 dark signal after electron beam irradiation.

Total dose (kGy)	Mean value (mV)/ $A=10^8$ V/A	Standard deviation (95 %)	Mean value (mV)/ $A=10^8$ V/A	Standard deviation (95 %)	Mean value (mV)/ $A=10^8$ V/A	Standard deviation (95 %)	Change (%)
0	46.48	10.11	-	-	-	-	0
100	-	-	- 254.41	4.61	-	-	- 647.30
300	-	-	-	-	- 998.76	34.89	2248.62

Table 9. The change of the photodiode Ph6 dark signal after gamma irradiation.

Total dose (kGy)	Mean value (mV)/ A=10^6 V/A	Standard deviation (95 %)	Mean value (mV)/ A=10^6 V/A	Standard deviation (95 %)	Mean value (mV)/ A=10^6 V/A	Standard deviation (95 %)	Change (%)
0	45.54884	8.06928	-	-	-	-	0
90	-	-	-17.6151	5.2765	-	-	-138.67
190	-	-	-	-	- 69.29	3.89	- 252.12

3. Conclusions

The main results of the investigation are:

1. the dark current degradation is more significant for InGaAs photodiode than for Si photodiode;
2. the change of the dark current is more important in the case of electron beam irradiation as compared to the gamma-rays for large area Si photodiode than in the case of those used for communication applications when the degradation has similar values for both types of irradiation;
3. for InGaAs photodiodes the dark current change for the case of electron beam irradiation is about 8 times higher than in the case of gamma irradiation;
4. the degradation of the spectral responsivity for large area photodiodes is quite similar in the case of electron beam and gamma-rays irradiation, and a local drop of the responsivity can be noticed;
5. the spectral responsivity for the Si photodiodes decreases as much as 54 % for the large area detectors subjected to electron beam irradiation, and by 10 % for gamma-rays irradiation, for the maximum total irradiation doses;
6. in the case of small area Si photodiodes the spectral responsivity decreases by 43 % under electron beam irradiation.